Heliyon 9 (2023) e20001

Contents lists available at ScienceDirect

Heliyon

journal homepage: www.cell.com/heliyon

# Multi-temporal shoreline analysis and future regional perspective for Kuwait coast using remote sensing and GIS techniques

Ikram M.S. Al-Attar [a], Manar A. Basheer [b,*]

[a] Mathematics Department, Kuwait College of Science and Technology, Kuwait
[b] Marine Science Department, National Authority for Remote Sensing and Space Sciences, Egypt

ARTICLE INFO

*Keywords:*
Shoreline changes
Failaka island
Bubiyan island
Kuwait
DSAS
EPR

ABSTRACT

Coastal regions are of extraordinary significance for the financial and welfare of human communities. Unfortunately, coastal regions are naturally pressured by anthropogenic activities that increase their vulnerability. Hence, there is a drastic need to monitor coastal changes to protect and manage them sustainably. Since Kuwait's coast is inhabited by about 94% of the inhabitants and most of the metropolitan area and the urgent need for sustainable planning and management of Kuwait's coast, this paper aims to analyze the historical changes rate of Kuwait's coast and Kuwait islands over 40 years from 1980 to 2020 and to predict the future changes of the shoreline in 2035 using EPR model. The results show that the highest accretion rate of the shoreline is 32.79 m/year, while the lowest erosion rate is −23.45 m/year. EPR of the islands revealed a fluctuation between erosion and deposition at each island. The future predicted shoreline changes were also mapped for the shoreline and islands.

## 1. Introduction

The shoreline is subject to irregular change due to morphological, climatic, or geological variables [1]. The energetic interfaces among tides, waves, rivers, storms, and tectonic and physical processes establish the coastline characteristics [2]. Coastline calculations are one of the essential techniques to estimate coastal erosion and accretion and the analysis of coastal morpho dynamics [3]. Because of its high accuracy, increased efficiency, and cost-effectiveness, remote sensing can monitor shoreline change in coastal areas more efficiently than conventional survey approaches [4,5]. Geographic Information Systems (GIS) technology allows users to visualize and simplify vast, complex data and produce high-quality maps. For instance, coastal changes brought on by the 2004 Tsunami are being studied in Banda Aceh and the neighboring areas using satellite imagery with high spatial and temporal resolution [6]. Several researchers [7–9] have addressed the global qualitative and quantitative study of shoreline spatiotemporal fluctuations. The shoreline change statistics rate is also determined using a time series of various coastline positions using the Digital Shoreline Analysis System (DSAS) extension tool. DSAS offers a complete set of regression rates in an easy-to-use technique that can be applied to massive amounts of data gathering at many scales. The software is suggested to provide rate-of-change data and the mathematical information required to ensure the reliability of the calculated results [10].

For the evaluation of shoreline positions over various periods, a variety of statistical change measures, such as Net Shoreline Movement (NSM), Shoreline Change Envelope (SCE), End Point Rate (EPR), Linear Regression Rate (LRR), and Weighted Linear

* Corresponding author.
*E-mail address:* mmanarmm2015@gmail.com (M.A. Basheer).

https://doi.org/10.1016/j.heliyon.2023.e20001
Received 15 November 2022; Received in revised form 7 September 2023; Accepted 7 September 2023
Available online 9 September 2023

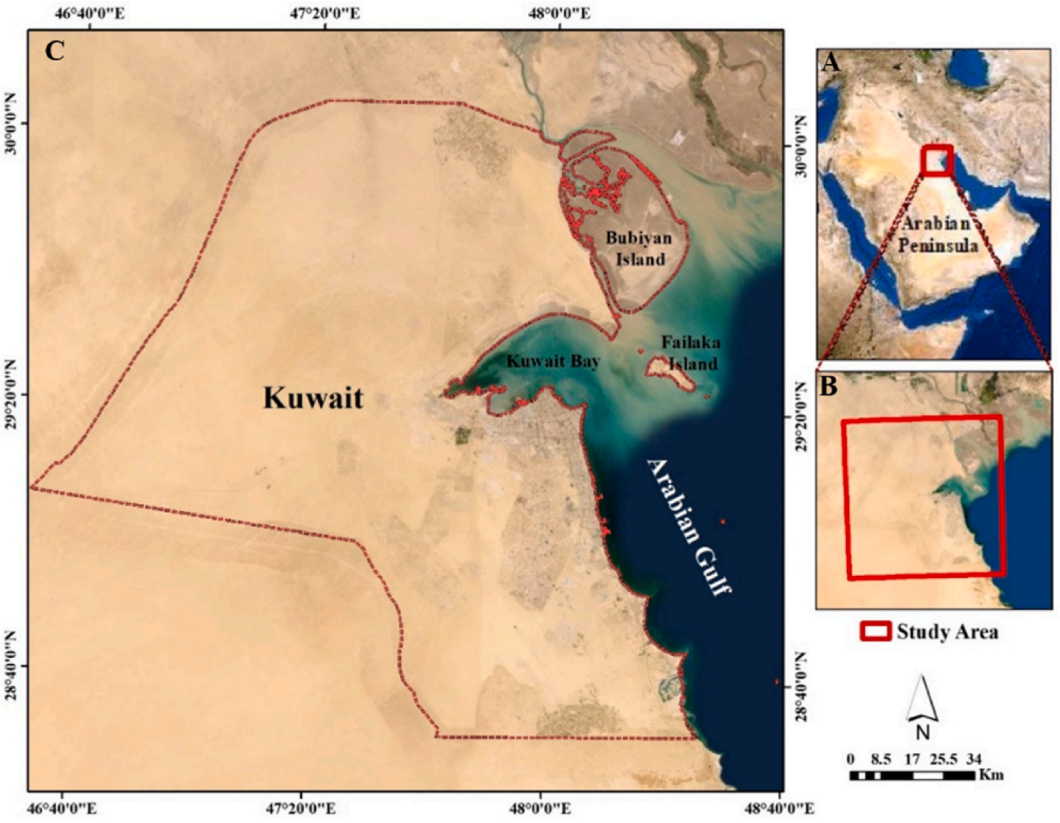


**Fig. 1.** Study area.

**Table 1**
Satellite images details.

| Satellite | Date of Acquisition | Spectral Resolution (meter) |
|---|---|---|
| Landsat MSS | 13/08/1980 | 60 m |
| Landsat TM | 13/01/1985 | 30 m |
| Landsat TM | 23/08/1990 | 30 m |
| Landsat TM | 21/08/1995 | 30 m |
| Landsat ETM+ | 11/09/2000 | 30 m |
| Landsat ETM+ | 09/09/2005 | 30 m |
| Landsat ETM+ | 12/12/2010 | 30 m |
| Landsat 8 OLI | 28/08/2015 | 30 m |
| Sentinel-2A | 27/09/2020 | 10 m |

Regression Rate (WLR), are derived within DSAS [11,12].

The endpoint rate (EPR) is measured by dividing the distance between the movement of the shoreline and the time elapsed between the oldest and the newest shoreline. The main advantage of EPR is the easy calculation, which requires at least two shorelines. Combining the EPR approach with satellite images is a precise and trustworthy process for calculating and analyzing shoreline change [13].

There is a great interest in coastal zones because nearly 66% of the world's population lives on coasts and areas less than 10 m above mean sea level [14]. Kuwait has a coastline of about 400 km, and 94% of the residents live in the coastal area [15]. Kuwaiti coast has a different coastal appearance, as it contains a variety of formations, such as mudflats, sabkhas, rocky headlands, artificial coasts, sandy coasts, and coastal cliffs. Understanding the amount of erosion and accretion and the spatial change is crucial for planning upcoming projects. Most of these features are due to increased and decreased sea levels; others, such as cliffs and plateaus, are primarily due to tectonic movements around the coastal region. Kuwaiti coasts are classified as complex coasts that are resulted from a combination of various factors [16]. Climate change-induced sea level rise threats the future socioeconomic development along Kuwait's coastline. The average annual temperatures will increase and are projected to reach a high of about 28.7 °C in Kuwait in 2035. This rise represents a 1.6 °C increase over the average annual temperature of the past decades. Therefore, it is essential to better understand Kuwait's vulnerability to climate change by monitoring shoreline changes and future predictions of the coastal area [17].

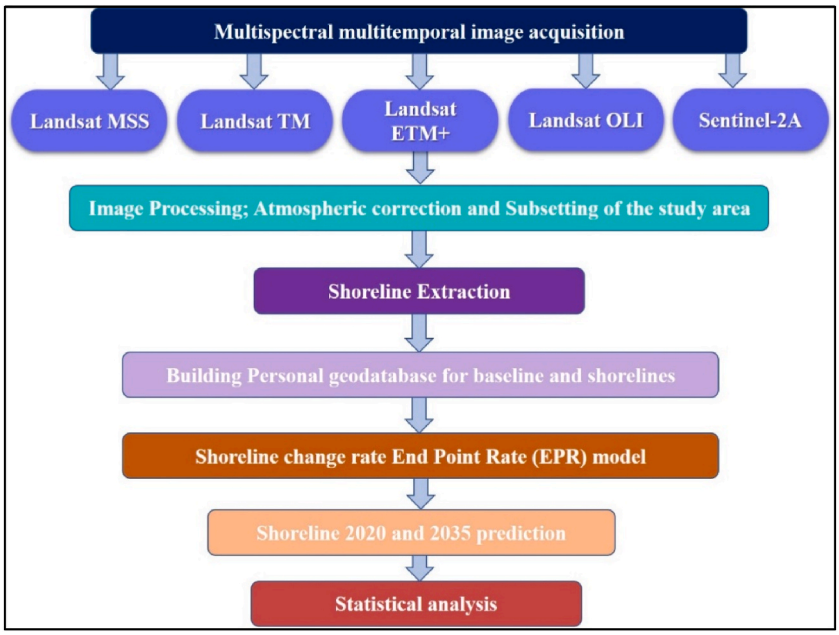


**Fig. 2.** Flowchart of the overall methodology applied in this study.

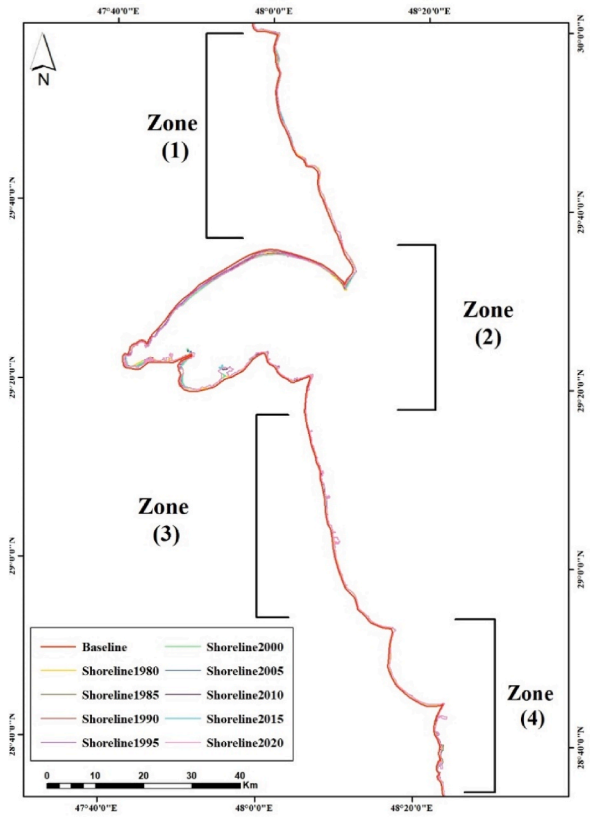


**Fig. 3.** Shoreline change of the study area (4 zones) from 1980 to 2020.

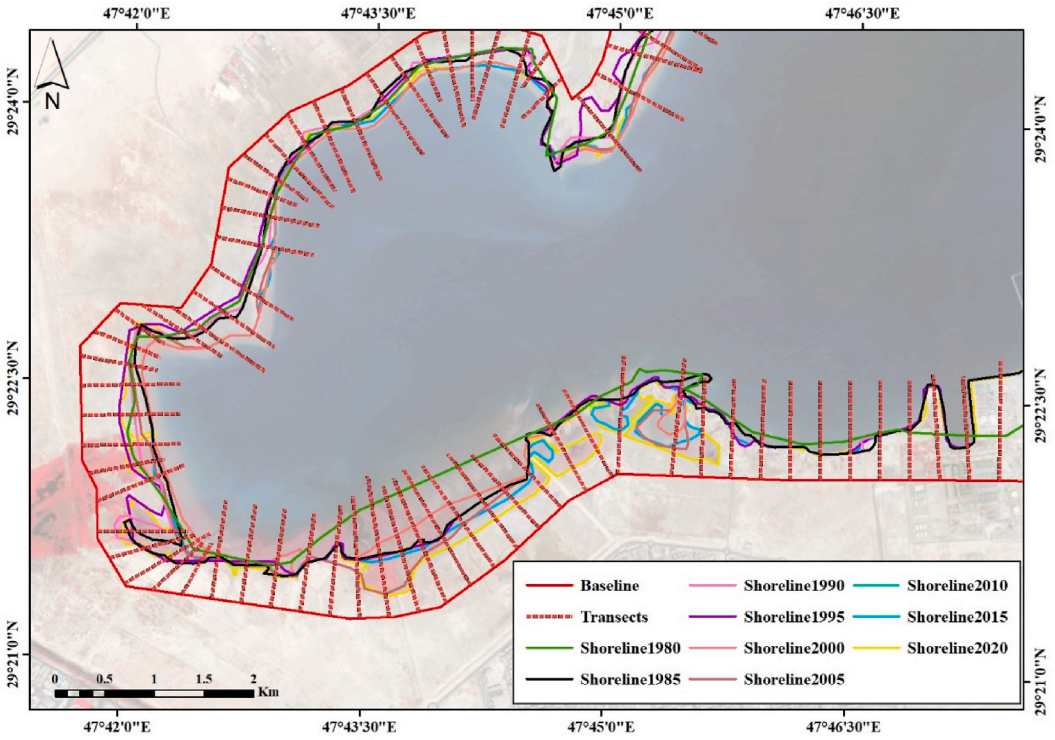


**Fig. 4.** Multitemporal shoreline positions, baseline, and transects used for calculation of EPR.

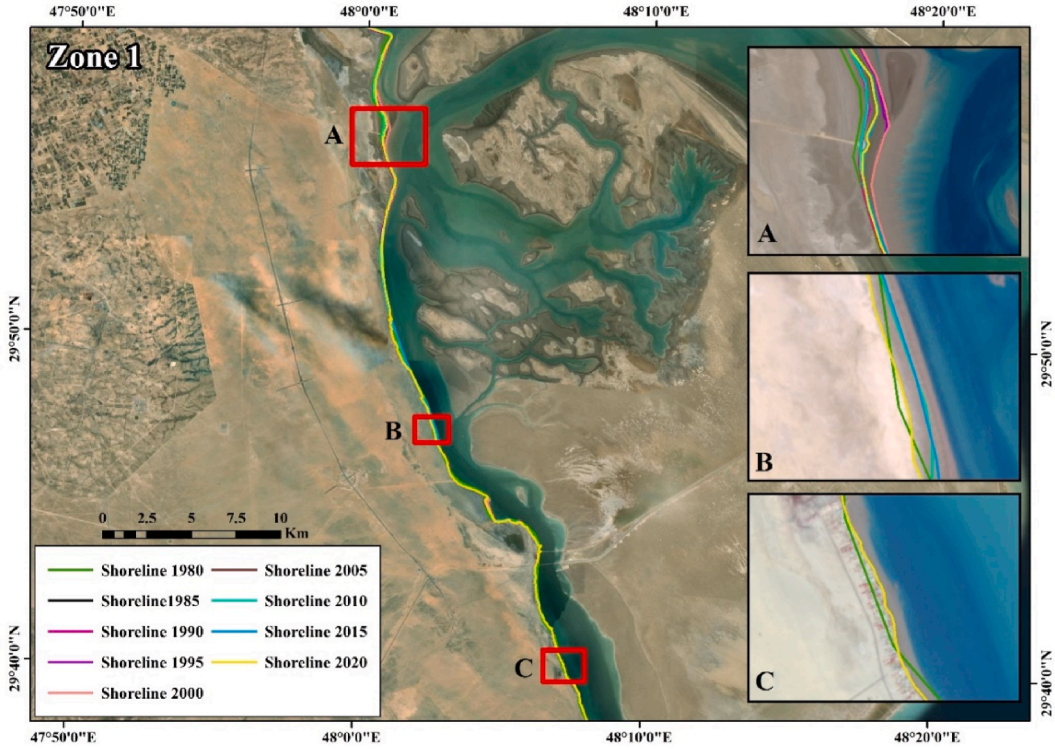


**Fig. 5.** Shoreline changes in different areas along zone 1.

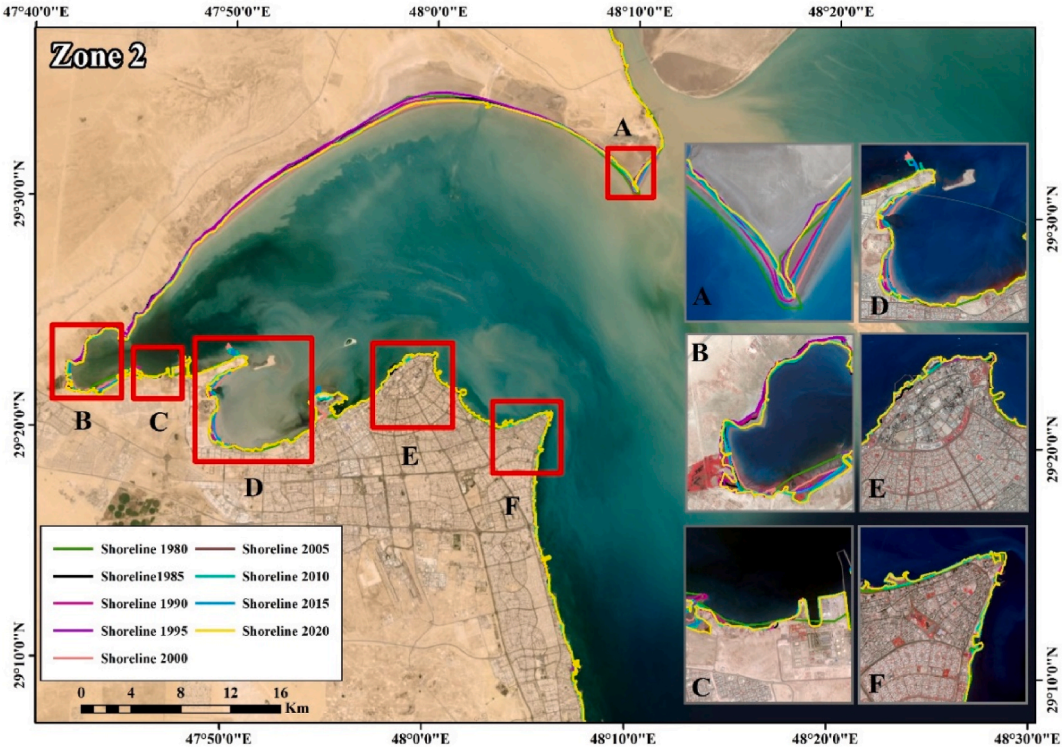


**Fig. 6.** Shoreline changes in different areas along zone 2.

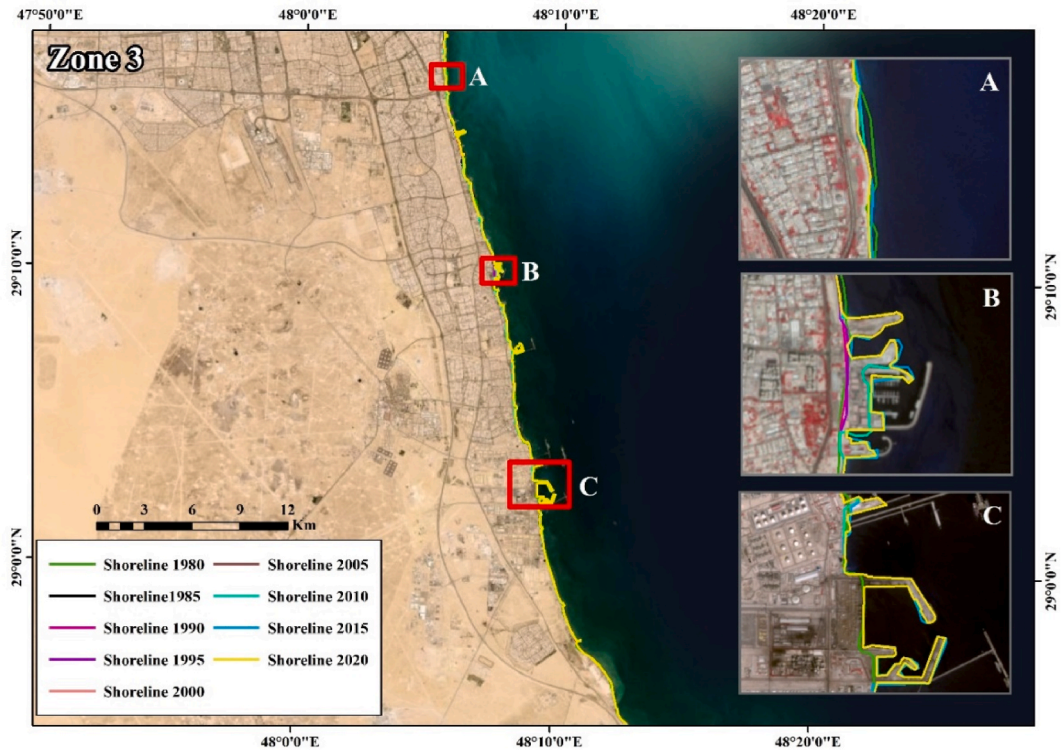


**Fig. 7.** Shoreline changes in different areas along zone 3.

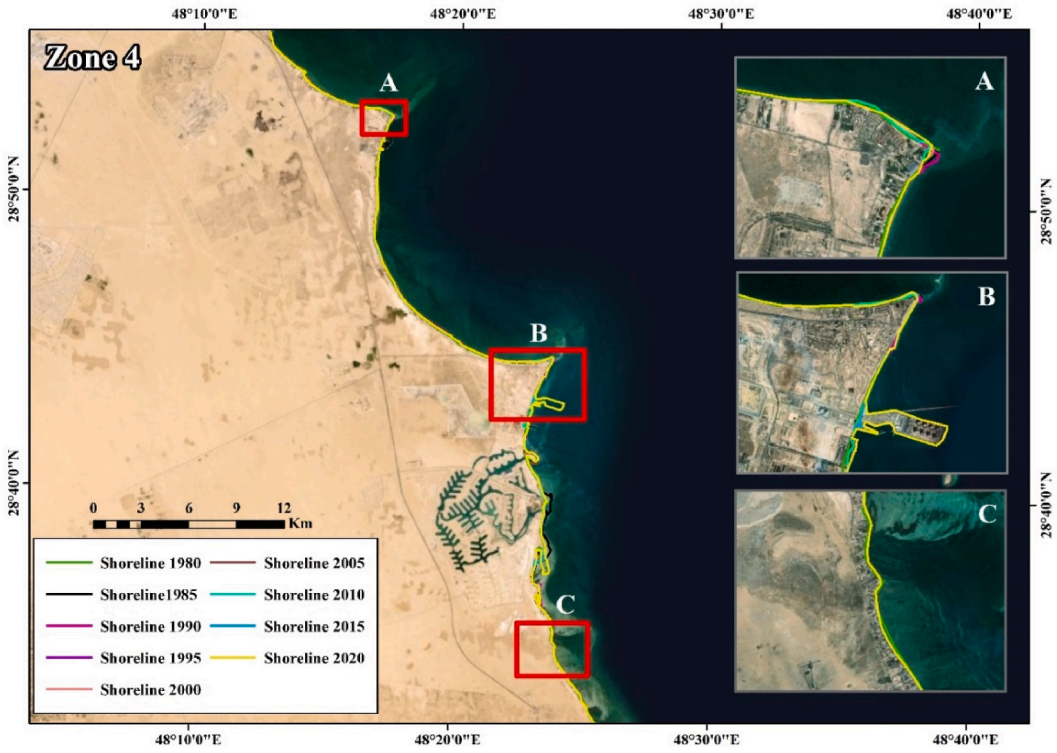


**Fig. 8.** Shoreline changes in different areas along zone 4.

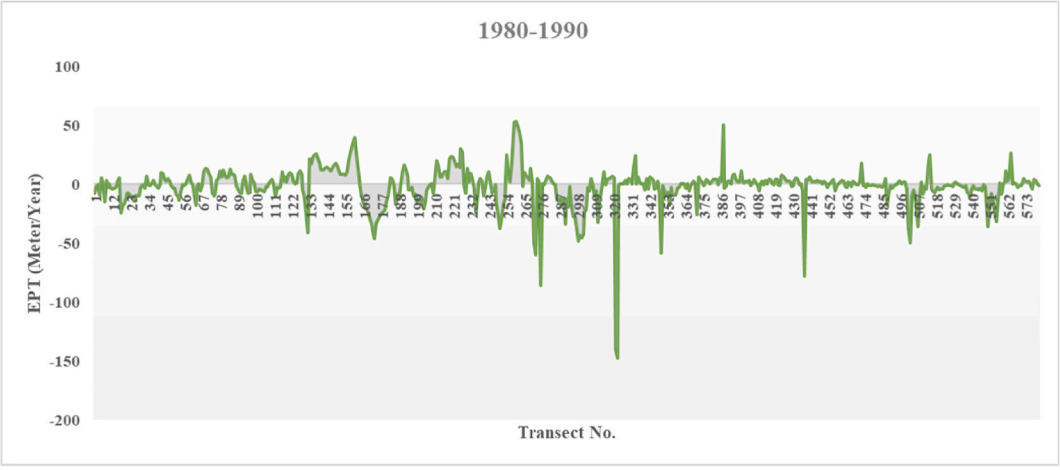


**Fig. 9.** Showing shoreline EPR from 1980 to 1990.

Coastal accretion or erosion is considered a hazard for infrastructure improvements in the coastal area. For instance, if a coastal area erodes the coastal infrastructure, such structures' foundations will be destroyed. On the other hand, if a coastal area is accreting, it will provide an expansive beach for recreation in certain areas. However, it is a hazard if sand accumulates around seawater intake structure sites; therefore, recognizing whether the Kuwaiti coast is historically eroding or accreting will aid in selecting an appropriate site for various coastal projects like harbors, ports, public beaches, desalination plants, etc. [18]. The study objectives are first to use multi-temporal satellite imageries to examine the variation in coastal erosion, accretion, and shoreline change over 40 years. The second objective is to analyze the Kuwaiti coast change rate and predict the future shoreline in 2035 to support decision-makers with the data for detecting suitable coastal zones for various upcoming coastal projects.

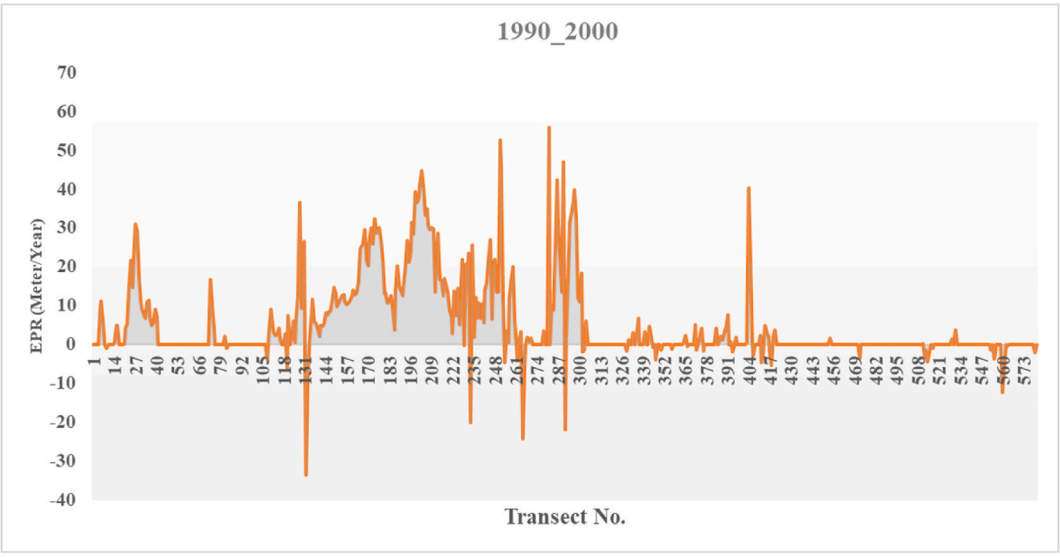


**Fig. 10.** Showing shoreline EPR from 1990 to 2000.

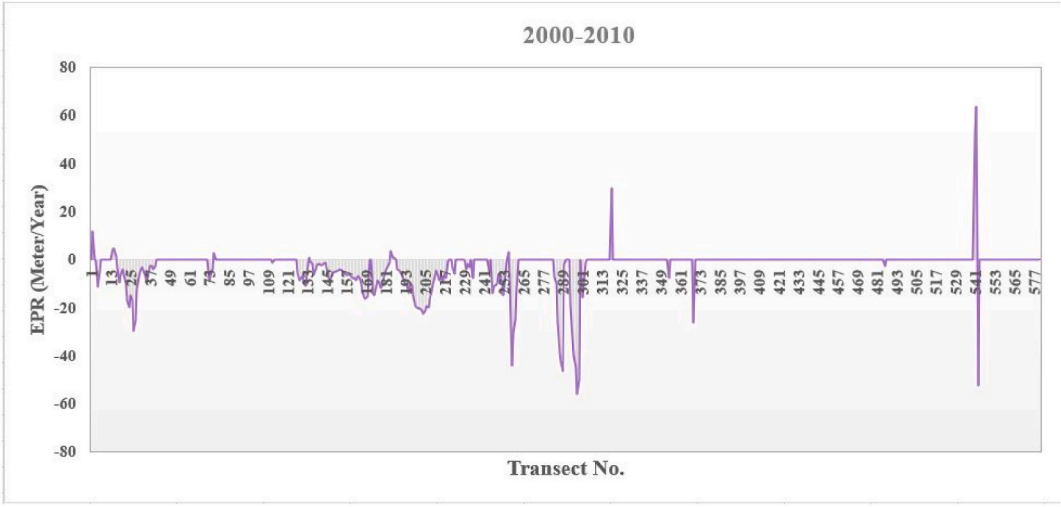


**Fig. 11.** Showing shoreline EPR from 2000 to 2010.

## 2. Material and methods

### *2.1. study area*

Kuwait is located between latitudes 28° 30′ and 30° 05′N and longitudes 46° 33′ and 48° 30′E; the Kuwaiti coast extends to about 415 km. Kuwait is enclosed by the Arabian Gulf from the East, Iraq from the North and West, and Saudi Arabia from the South, with an approximate area of 17,818 km$^2$ (Fig. 1(A-C)).

Kuwait Bay bathymetry consists of three physiographic categories.

(1) A submerged estuarine flat in the North,
(2) The Kuwait Bay trough in the centre, and (3) The sharp slope in the South.

Kuwait Bay's average depth is almost 5 m, while the most significant depth near Ras al Ardh is about 30 m [19].

Kuwait Bay is composed of muddy soil. Sandy soils are found near the narrow southern offshore flat and the western and eastern parts of the central flat [20]. Kuwait's territorial waters cover 7611 km$^2$; this water can be separated into shallow northern water, which has a depth of less than 5 m and has a muddy bed, and the comparatively deep southern area, which contains a sandy bed with

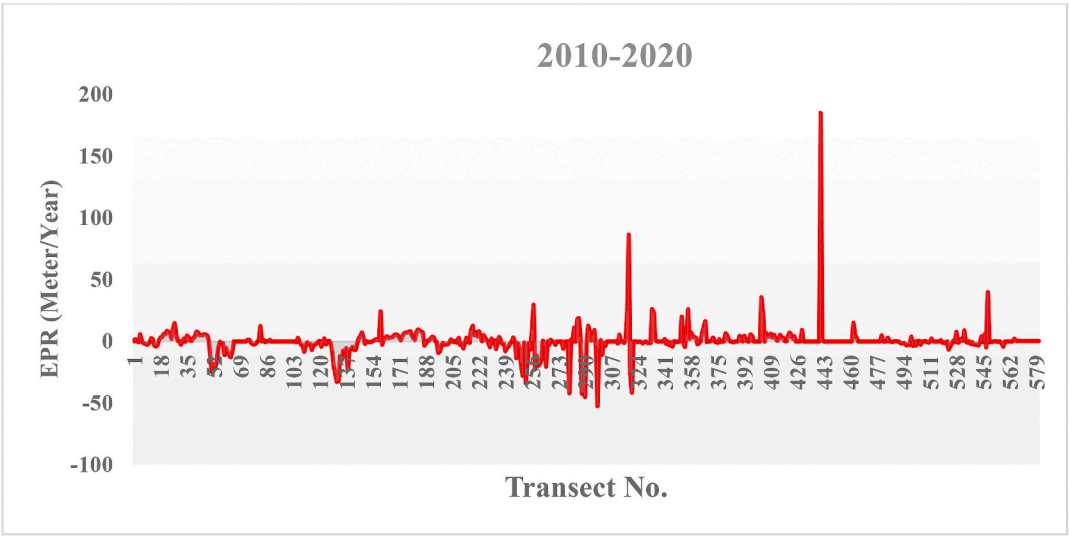


**Fig. 12.** Cart showing shoreline EPR from 2010 to 2020.

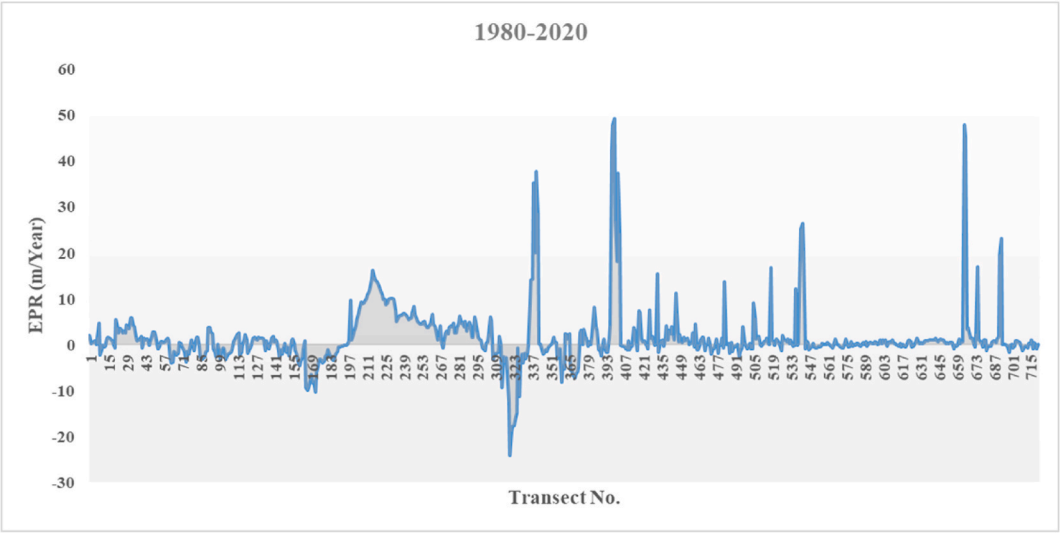


**Fig. 13.** Showing shoreline EPR from 1980 to 2020.

**Table (2)**
Zone wise shoreline change rate using EPR.

| No. | Zones Characteristics | Zone 1 | Zone 2 | Zone 3 | Zone 4 |
|---|---|---|---|---|---|
| 1 | Total Number of Transect | 130 | 235 | 117 | 98 |
| 2 | Shoreline length (km) | 69.88 | 161.62 | 79.13 | 61.94 |
| 3 | Mean erosion rate (m/year) | −1.64 | −3.47 | −0.68 | −0.58 |
| 4 | Mean accretion rate (m/yr.) | 1.75 | 5.60 | 2.19 | 3.02 |
| 5 | Mean shorelines change rate (m/year) | 0.19 | 2.04 | 0.74 | 1.72 |
| 6 | Shoreline Change Rate (minimum) | −4.75 | −23.45 | −4.47 | −2.79 |
| 7 | Shoreline Change Rate (maximum) | 5.49 | 27.36 | 21.4 | 32.79 |
| 8 | Total Transect that Record Erosion | 60 | 91 | 59 | 35 |
| 9 | Total Transect that Record accretion | 70 | 144 | 58 | 63 |
| 10 | Zone wise overall trend | Accretion | Accretion | Accretion | Accretion |

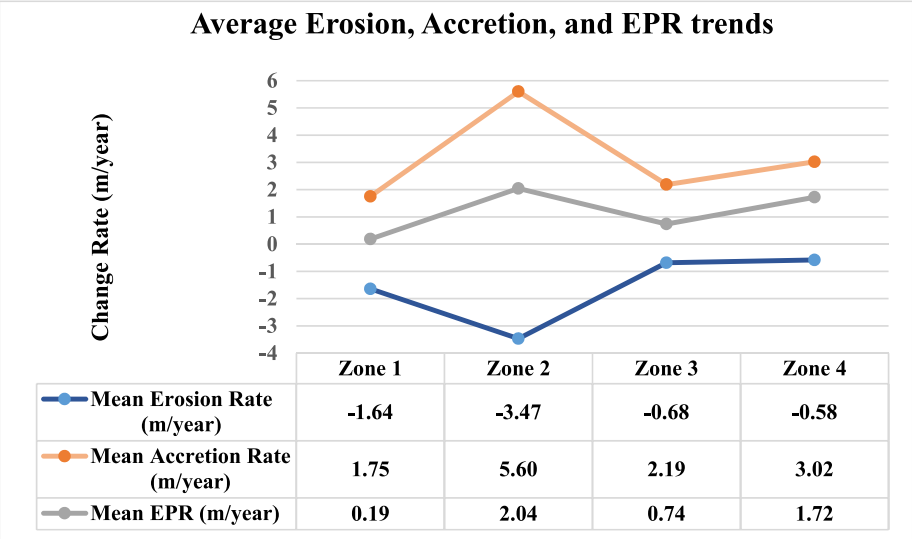


| | Zone 1 | Zone 2 | Zone 3 | Zone 4 |
|---|---|---|---|---|
| Mean Erosion Rate (m/year) | -1.64 | -3.47 | -0.68 | -0.58 |
| Mean Accretion Rate (m/year) | 1.75 | 5.60 | 2.19 | 3.02 |
| Mean EPR (m/year) | 0.19 | 2.04 | 0.74 | 1.72 |

**Fig. 14.** Average trends of erosion, accretion and EPR in Kuwaiti coast.

silica deposits [21]. The tidal cycle in Kuwait Gulf is classified as semidiurnal, where the tidal period is 12 h and 25 min. The range of the tide is about 4 m. The sediments on the North of Kuwait Bay coast are muddy, while the sediments on the South are rocky and sandy. The Bathymetry varies from 5 m to 26 m in the Kuwait Gulf [22]. A flat coastal plain defines Kuwait's topography [23]. Kuwait's coastal region is home to three sedimentary formations: The Ghar and Fars formations, the Pleistocene formations, and the Holocene formations. The Three types of sediments comprise Kuwait's coastal region, with proportional areas comprising 28, 22.9, and 49.1% of the total coastal region area. The loose and delicate sandy deposits that make up these formations are particularly prone to coastal erosion because of sea level rise, stronger waves, and accelerated decay (weathering) processes [24]. Kuwait's coastline typically has mild, gradual slopes, accounting for 40.1% of the total slope, with an average slope of about 4.8°. The coastline sediment grain size is divided into four types of beaches: sandy, rocky, muddy, and sandy muddy, representing 40.3%, 28.5%, 23.6%, and 7.6% of the total area of natural beaches, respectively [25]. The northern coastline, which surrounds Kuwait Bay and Khor Sabiya, and the southern coastline, which runs along the Arabian Gulf, can be classified as the coastal zone of Kuwait state. Sandy beaches characterize the coastline of Kuwait Bay, while Khor As -Sabiya features vast intertidal mudflats, sandy beaches, rocky outcrops, and saline marshes. Sandbars, tide inlets, cliffs, and coastal dunes comprise most of the southern shoreline. The soft mud dominates all Bubiyan island boundaries [26].

### 2.2. *Bubiyan Island*

The largest island in Kuwait is Bubiyan Island, which encompasses an area of almost 1200 $km^2$ (almost 7% of Kuwait). This island is isolated from the mainland (to its west) by Khor as Subiyah (maximum 3 km wide). It is bordered by Khor Bubiyan (1.5–2 km wide) in the north and Khor Abdullah in the east (3 km wide in Kuwaiti regional waters). The southern edge of Bubiyan island faces the Arabian Gulf, with muddy beaches (almost 2 km wide) found on the island's eastern and southern coasts [27].

Bubiyan Island, which covers an area of about 900 $km^2$, is located in Kuwait in the northwestern corner of the Arabian Gulf. It is far from the Kuwaiti mainland, about 2 km, separated by the Subbiyah Khor. Bubiyan island is exposed to flood by rainwater and sea tides and climatic changes seasonally. The soft mud dominates all Bubiyan island boundaries except a few sand mounds that characterize the southern coastal area of the island; the northern portion is home to a distinctive network of tidal waterways that includes salt marsh wetlands of regional significance [28].

### 2.3. *Failaka Island*

Failaka Island is an elliptically shaped island in the northwestern part of the Arabian Gulf and outside Kuwait Bay. This island is located at 29°26′20″ N and 48°20′00″ E. It is the second largest island of Kuwait, located on the downstream side of Shatt Al-Arab, about 20 km away from Kuwait's coastline, with a length of approximately 12 km, a width of about 6 km, and a total area of 43 $km^2$. The island is flat except for a little slope on its western side, about 9 m high. Failaka Island was created by the structural expansion of the Jal Al-Zour, an enlarged bank of the Khor Subbyia made of secondary pebbles and sand from the Neogene period [29].

The island has a hot, dry climate with moderate winds. In the summer, the temperature can get as high as 50 °C, while in the winter, it can get as low as 4 °C. On the island, average monthly wind speeds range from 3 to 7 m/s. Moreover, 130 mm of rain precipitation occurs yearly [26].

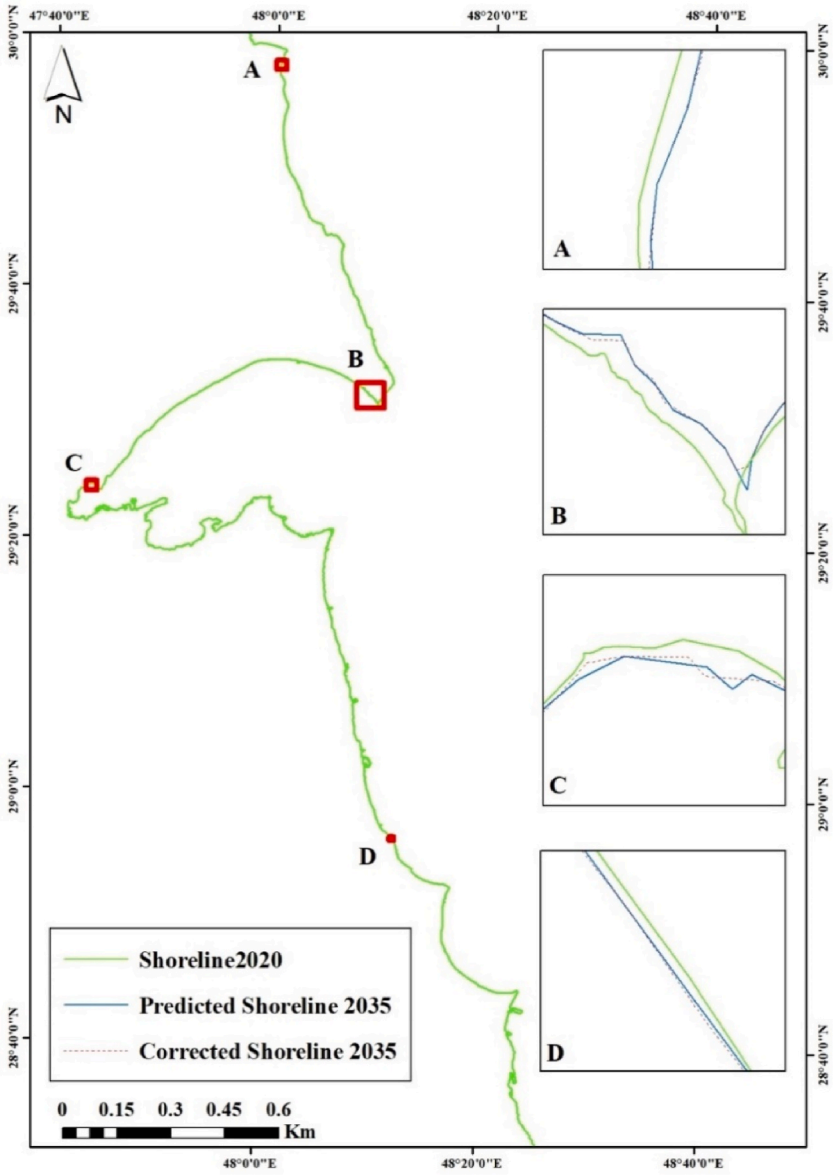


**Fig. 15.** Predicted and corrected Shoreline 2035.

### *2.4. Data*

Multi-temporal satellite imageries of Landsat MSS, TM, ETM, OLI, and Sentinel-2A (Table 1) have been utilized for the study area in 1980, 1985, 1990, 1995, 2000, 2005, 2010, 2015, and 2020, with UTM (Universal Transverse Mercator) zone 39 (WGS-84) projection. The Kuwait shoreline change analysis study has followed the methodology workflow shown in Fig. 2.

### *2.5. Shoreline extraction and change rate calculation using EPR from 1980 to 2020*

A transect layer was created in which the distance between transects was 500 m. The multi-date (1980–2020) shorelines were extracted through the on-screen digitization of satellite images of distinct periods using ArcGIS to extract all required shorelines.

The study area was divided into four zones (1–4) (Fig. 3). The Digital Shoreline Analysis System (DSAS) tool was used to estimate the shoreline change rate.

In this study, DSAS is performed in five stages: shorelines extraction, baseline creation, transects generation, calculation of distances between baseline and shorelines at each transect, and calculation of the rate of shoreline change [30]; Nassar et al., 2018). DSAS requires that the feature class have specific attribute fields; OBJECTID, SHAPE, SHAPE Length, DATE_, and UNCERTAINTY. Users have

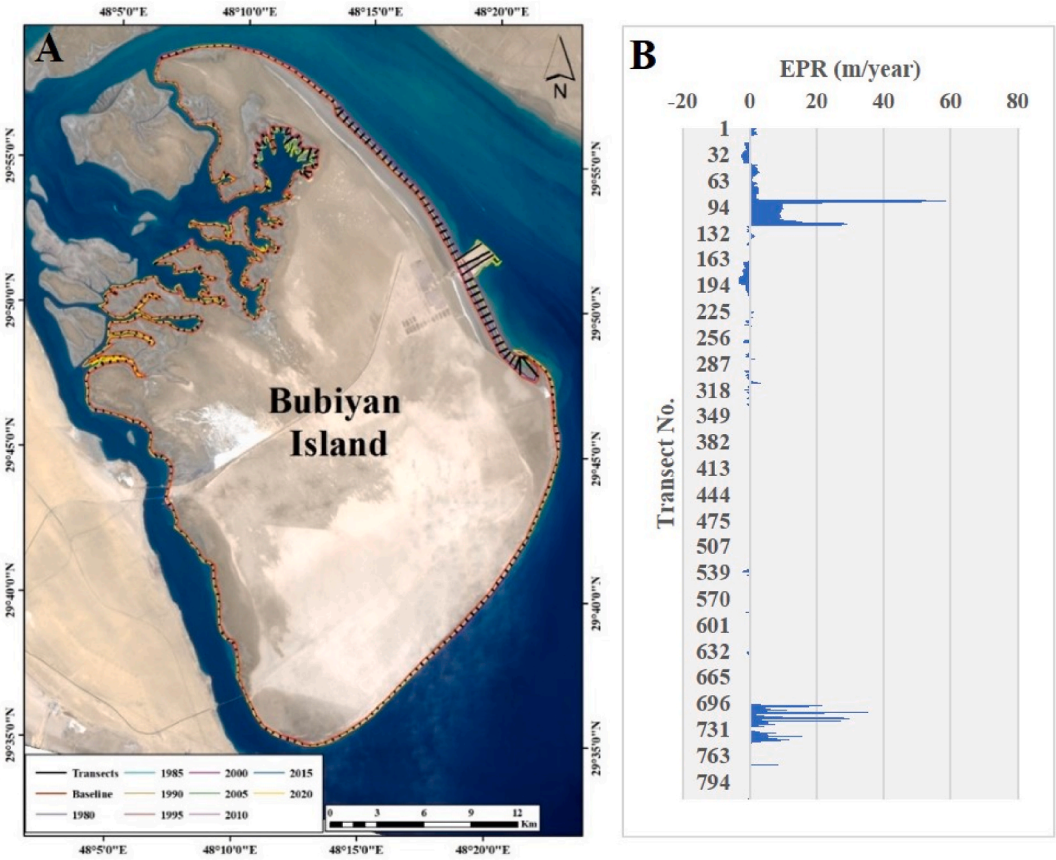


**Fig. 16.** Multitemporal shoreline position of Bubiyan island from 1980 to 2020 with transects with EPR.

the option of adding to each shoreline an overall uncertainty value. Otherwise, DSAS will use the value in the Set Default parameters window. DSAS determined all required data from the input baseline, shoreline, and transect files covering the entire coastal waters of Kuwait from the southern region to the northern region, as shown in Fig. 4. The concept of rate calculation relied on calculating the differences between shorelines through time. Agreeing with [31]; EPR could be a straightforward and helpful process for anticipating shoreline alter rate. Within the (EPR), the average yearly rate of shoreline alteration is calculated by separating the removal of shoreline development by the time distinction between the shoreline of the primary date and the final date, as adjusted by Ref. [32]. DSAS computes the shoreline alter rate for a time arrangement through 6 strategies, and EPR is one of them [33]. The main points of this strategy are the effortlessness of computation and the negligible requirement for, as it were, two shorelines. The yearly shoreline alters rate was assessed for interims as takes after; 1980–1990, 1990–2000, 2000–2010, and 2010–2020 utilizing the EPR strategy.

### *2.6. Prediction of shoreline*

The future shoreline was predicted using the shoreline change rate, the time interval between actual and predicted shoreline and intercept, according to the following equation:

Future shoreline = (time interval * shoreline change rate) + intercept.

At first, the model was adjusted based on 1980, 1985, 1990, 1995, 2000, 2005, 2010, 2015, and 2020 shorelines. Also, the study area's 2010, 2015, and 2020 shorelines were used to predict 2035. The predicted shoreline for 2035 was adjusted by calculating the Root Mean Square Error (RMSE) was calculated, which depends on the actual 2020 shoreline that is obtained from the 2020 Sentinel-2A image and the other predicted one, which is calculated using the actual shores of 2010, 2015 and 2020 shorelines. In this study, 10 m uncertainty for each shoreline is set by USGS as part of the prediction to create an uncertainty region that lies within a 95-percent confidence interval [34,35].

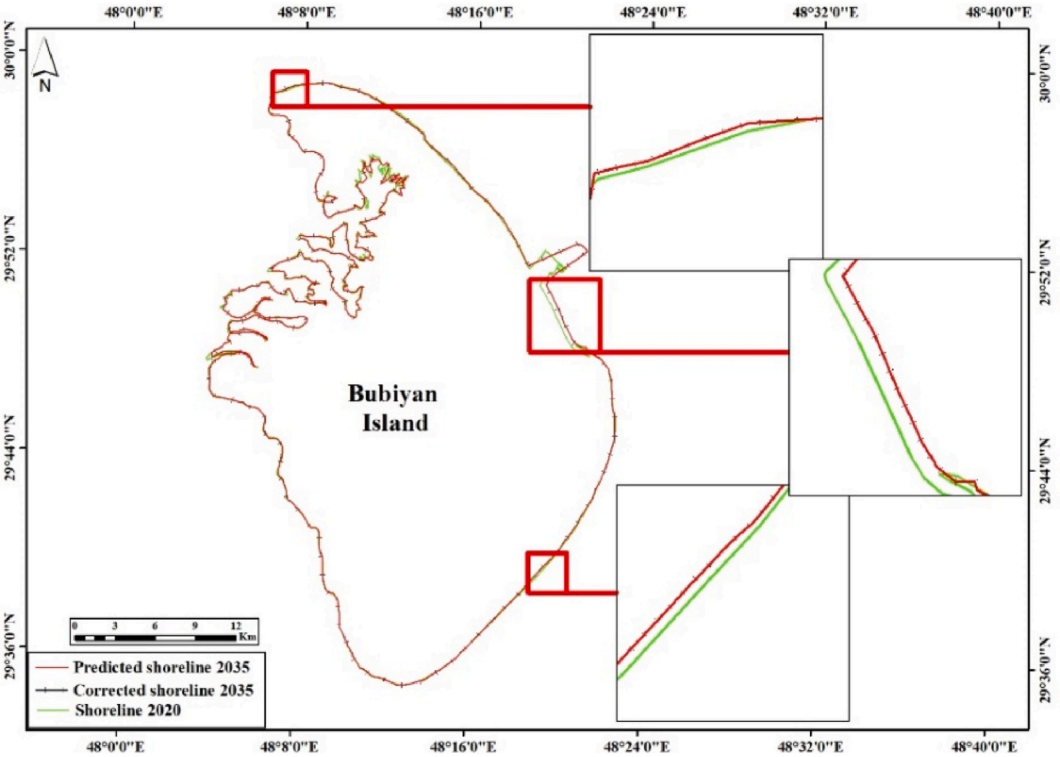


**Fig. 17.** Predicted and corrected Shoreline 2035 of Bubiyan island.

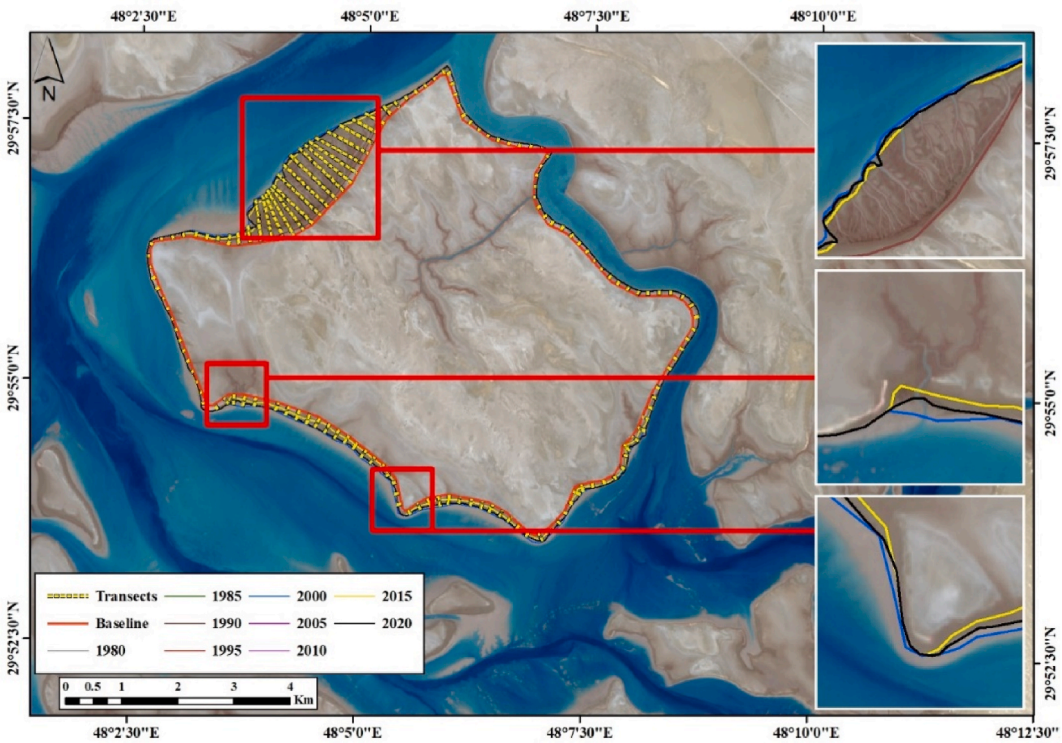


**Fig. 18.** Multitemporal shoreline position of Warbah island from 1980 to 2020 with transects.

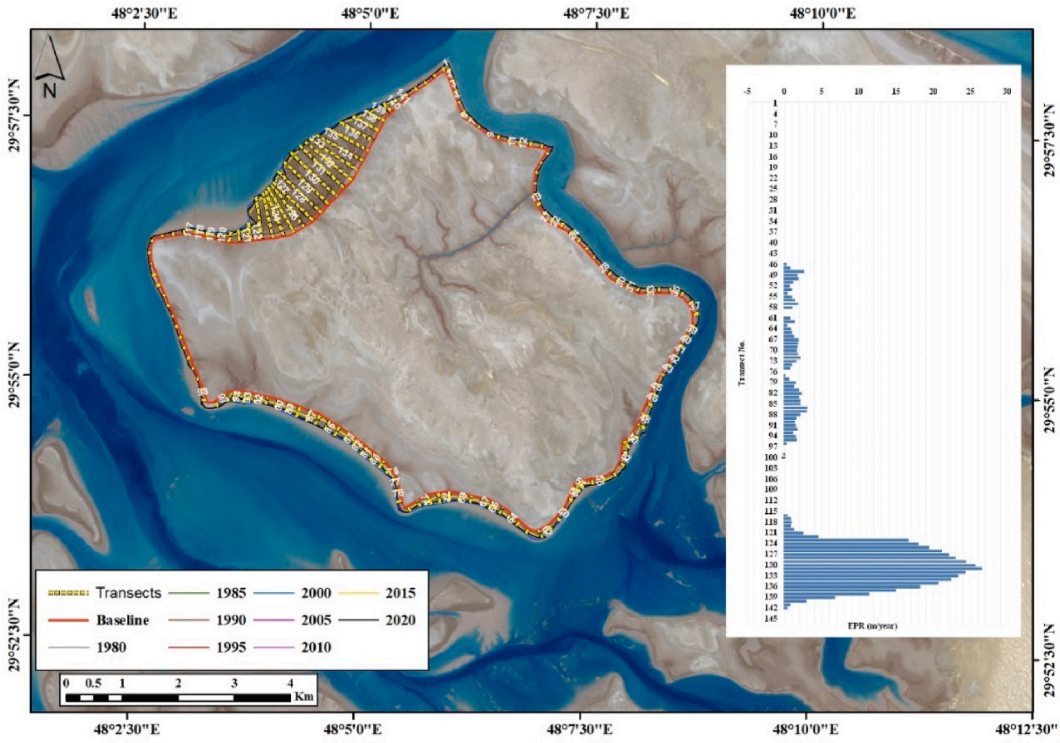


**Fig. 19.** EPR from 1980 to 2020 of Warbah island.

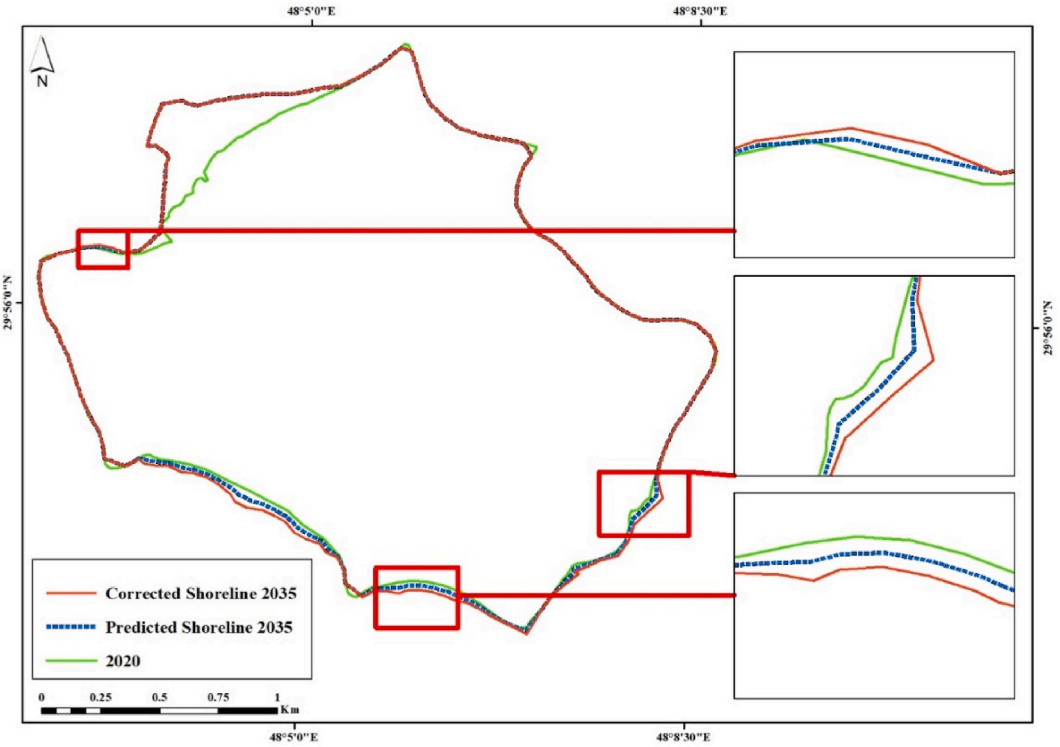


**Fig. 20.** Predicted and corrected Shoreline 2035 of Warbah island.

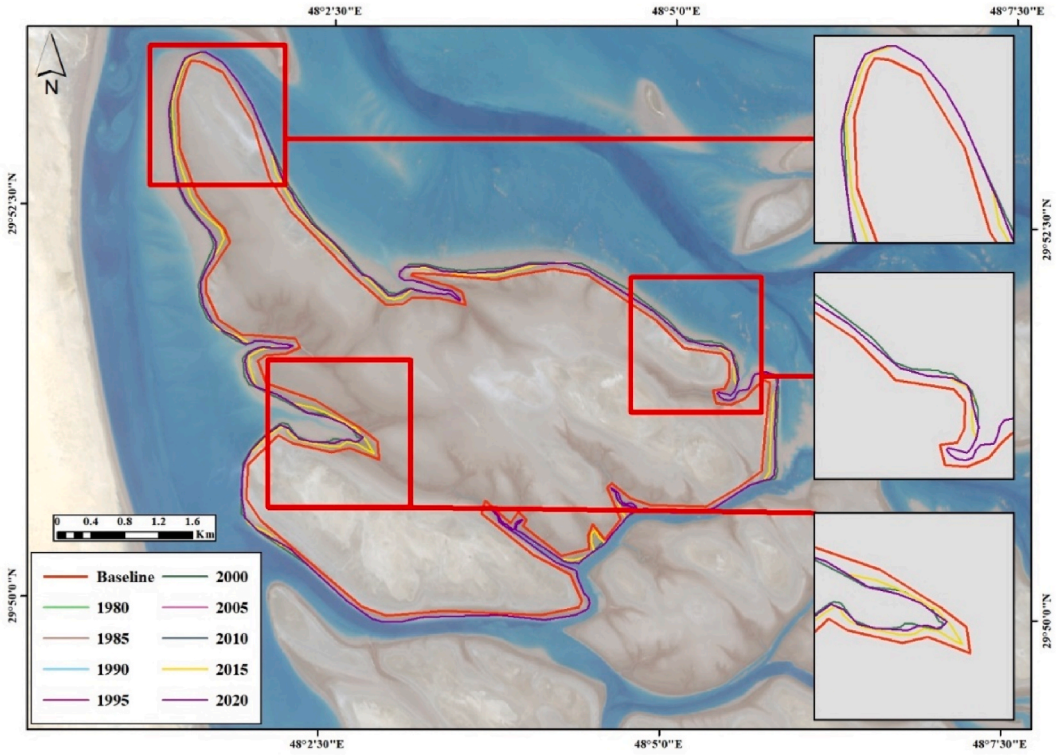


**Fig. 21.** Multitemporal shoreline position of second detached island from 1980 to 2020.

## 3. Results and discussion

### *3.1. Shoreline changes in Kuwait shoreline during the period 1980–2020*

The shoreline of the Kuwaiti coast extraction was extracted using the digitization method from 1980 to 2020 (Fig. 5(A-C), 6(A-F), 7 (A-C), 8(A-C)). Fig. 5A-C shows shoreline changes in different areas along Zone 1; Zone 1 is exposed to erosion in most of the coast due to the nature of the coast, which is sandy in the north and muddy in the south. Fig. 6(A-F) shows shoreline changes in different areas along zone 2, representing Kuwait Bay; area A characterized by sandy soil and experienced erosion, while area B shows shoreline erosion due to muddy soil. Areas C, E, and F, characterized by rocky soil, show more minor changes than the others. Area D shows shoreline erosion because of the sandy soil. Fig. 7(A-C) shows shoreline changes in different areas along zone 3 and comprises different port areas; all the represented areas A, B, and C are characterized by sandy soil, showing shoreline erosion except at areas where ports were constructed. Fig. 8(A-C) shows shoreline changes along zone 4, representing Kuwait's south coast. The three represented areas are characterized by rocky soil showing low shoreline changes. Change rates were calculated between 1980 and 1990, 1990–2000, 2000–2010, 2010–2020, and 1980–2020 then illustrated in figures 9–13. These figures show that the time interval from 1990 to 2000 was the highest accretion rate of the shoreline compared to the other time intervals, and from 2000 to 2010, the shoreline was exposed to the highest erosion rate. The results show that zone 1 of the coast that faces Bubiyan island (from Transect 1 to 130) has a maximum accretion rate of 5.49 m/year in transect number 27 and an average accretion rate of 1.75 m/year and a minimum erosion rate of −4.75 m/year in transect number 128 and average erosion rate −1.64 m/year. Zone 2, which represents Kuwait Bay (from transect 131 to 365), has a maximum accretion rate of 27.36 m/year in transect number 272, an average accretion rate of 5.6 m/year, and a minimum erosion rate of −23.45 m/year in transect number 258 and average erosion rate −3.47 m/year. Zone 3 (from transect 366 to 482) has a maximum accretion rate of 21.4 m/year in transect number 436, an average accretion rate of 2.19 m/year, and a minimum erosion rate of −4.47 m/year in transect number 471 and average erosion rate −0.68 m/year. In comparison, zone 4 (from transect 483 to 580) has a maximum accretion rate of 32.79 m/year in transect number 559, an average accretion rate of 3.02 m/year, and a minimum erosion rate of −2.79 m/year in transect number 548 and average erosion rate −0.58 m/year. Zone 2 has the highest shoreline change rate compared to the other zones along the coast. Table 2 shows that Zone 1 has 130 transects with a coastal length of 69.88 km, while Zone2 has 235 transects and covers 161.62 km of the coast, zone 3 includes 117 transects with 79.13 coastal length, and Zone 4 has only 98 transects and cover 61.94 km. The mean accretion rate for zones 1, 2, 3, and 4 are 1.75, 5.60, 2.19, and 3.02 m/year, respectively. The mean erosion rate for zones 1, 2, 3, and 4 are −1.64, −3.47, −0.68 and −0.58 m/year. The maximum mean EPR is found along Zone 2 (2.04 m/year), while zone 1 has shown a minimum EPR (0.19 m/year) (Fig. 14) (Table 2). The EPR method has been used to predict of future shorelines in 2020 and 2035, Fig. 15(A-D). The predicted shorelines revealed that the accretion and

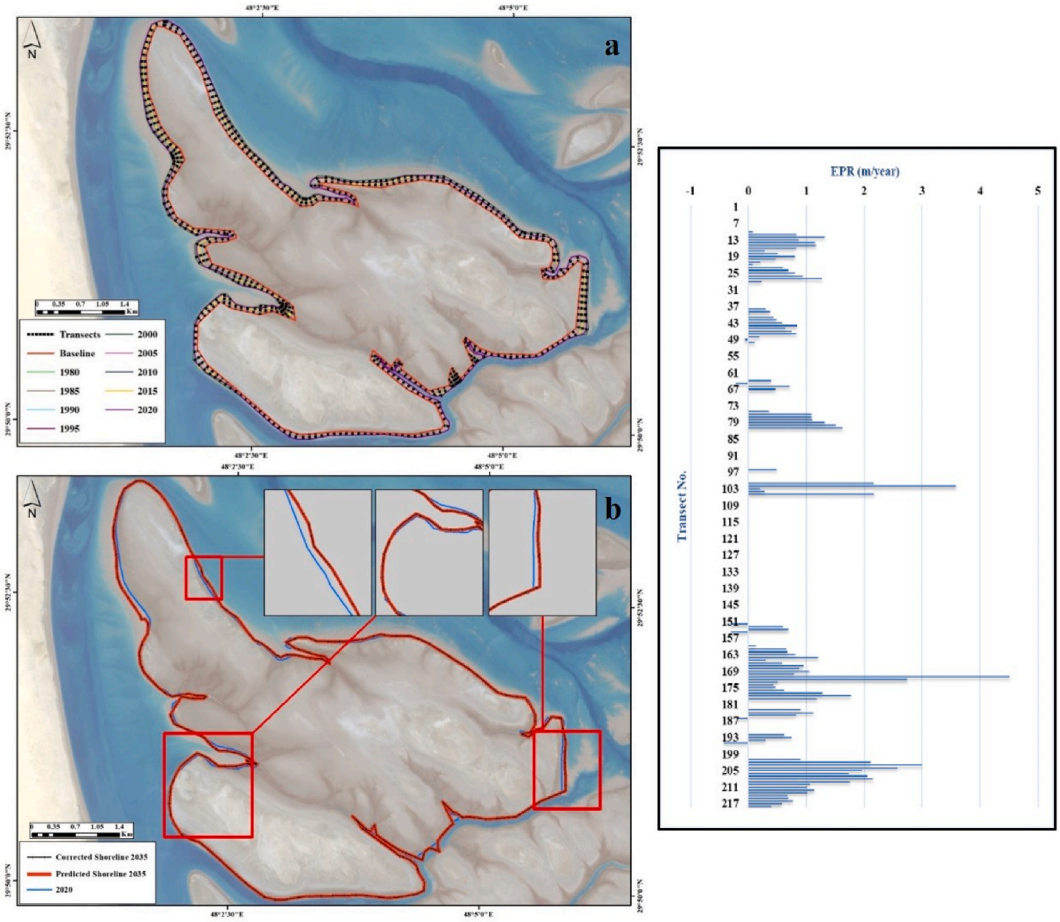


**Fig. 22.** a) EPR from 1980 to 2020 of second detached island, b) Predicted and corrected Shoreline 2035.

erosion along the Kuwaiti coast would be negligible except for zone B, which will undergo the highest change rate.

### *3.2. Shoreline changes in Bubiyan Island and prediction of future shoreline*

The result of the transect analysis with the EPR method is shown in Fig. 16(A-B). The results show that Bubiyan island has a maximum accretion rate of 62.3 m/year in transect number 45 due to the construction of the port, an average accretion rate of 2.23 m/year, and a minimum erosion rate of −19.8 m/year in transect number 373 and average erosion rate −2.03 m/year. Fig. 17 shows the predicted and corrected Shoreline 2035 of Bubiyan Island.

### *3.3. Shoreline changes in small islands that detached from Bubiyan islands and prediction of future shoreline*

The result of the transect analysis with the EPR method for Warbah Island is shown in Figs. 18 and 19. The results show that the island has a maximum accretion rate of 1.51 m/year in transect number 131, an average accretion rate of 2.89 m/year, a minimum erosion rate of −0.31 m/year in transect number 100, and an average erosion rate of −0.14 m/year. Figs. 18 and 19 reveal that the upper side of this island has the highest accretion rate compared to the other sides. Fig. 20 shows the predicted and corrected Shoreline 2035 of Warbah Island.

The result of the transect analysis with the EPR method for the second detached island is shown in Figs. 21 and 22a. The results show that the island has a maximum accretion rate of 4.52 m/year in transect number 171, an average accretion rate of 0.43 m/year, and a minimum erosion rate of −0.42 m/year in transect number 195, and an average erosion rate of −0.25 m/year. Fig. 22b shows the second detached island's predicted and corrected Shoreline 2035.

The result of the transect analysis with the EPR method for the third and fourth detached islands is shown in Fig. 23a. The results show that the third has an accretion rate of 0–2.98 m/year and an average accretion rate of 0.43 m/year. The results show that the fourth has a maximum accretion rate of 5.67 m/year in transect number 9, an average accretion rate of 2.59 m/year, and a minimum erosion rate of −1.79 m/year in transect number 1, and an average erosion rate of −1.47 m/year. Fig. 23b shows the second detached

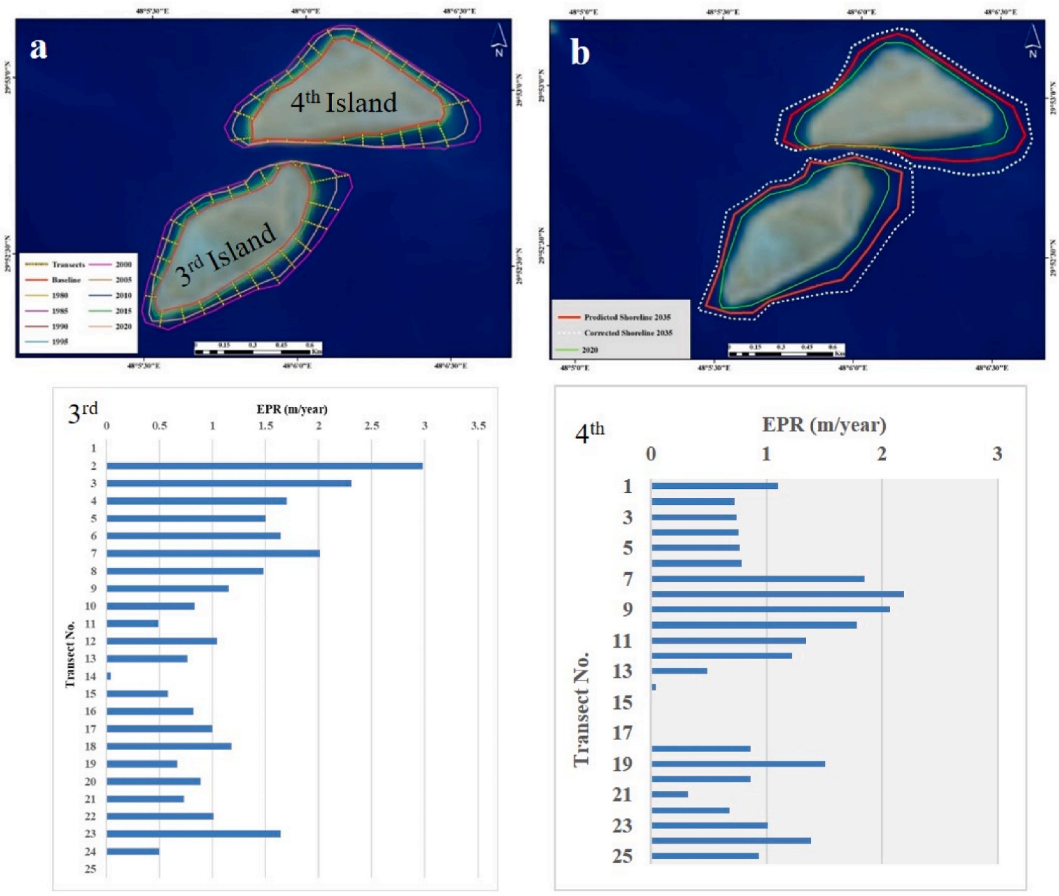


**Fig. 23.** a) Multitemporal shoreline position of third and fourth detached island from 1980 to 2020 with transects with EPR, b) predicted and corrected Shoreline 2035.

island's predicted and corrected Shoreline 2035.

The result of the transect analysis with the EPR method for the fifth detached island is shown in Fig. 24a. The results show that the island has an accretion rate of 0.0–1.34 m/year and an average of 0.54 m/year. Fig. 24b shows the second detached island's predicted and corrected Shoreline 2035.

### *3.4. Shoreline changes in Failaka Island and prediction of future shoreline*

The result of transect analysis with the EPR method is shown in Figs. 25 and 26. The results show that Failaka island has a maximum accretion rate of 5.68 m/year in transect number 22, an average accretion rate of 0.18 m/year, and a minimum erosion rate of −1.47 m/year in transect number 24, and an average erosion rate of −0.46 m/year. Fig. 27 shows the predicted and corrected Shoreline 2035 of Failaka Island.

## 4. Conclusion

Every country with a coastline must study the coast dynamic and the shoreline changes over a prolonged period. Erosion and accretion are common coastal phenomena. Shoreline changes analysis from 1980 to 2020 along the coast of Kuwait, utilizing GIS and statistical techniques, has participated in better recognition of the dynamic of the coast by identifying the areas of accretion and erosion. Shoreline changes were extracted using the EPR model over 40 years, revealing that the shoreline fluctuated between erosion and accretion at different rates. The future predictions of shoreline position clarified that the areas of the shoreline that will be exposed to tremendous loss by erosion would be provided urgently. This method will aid in mapping the best scenario for the sustainable development of coastal areas, selecting the most suitable areas for the construction of incoming projects, and warning decision-makers to develop appropriate strategies for adaptation, especially in vulnerable or threatened areas.

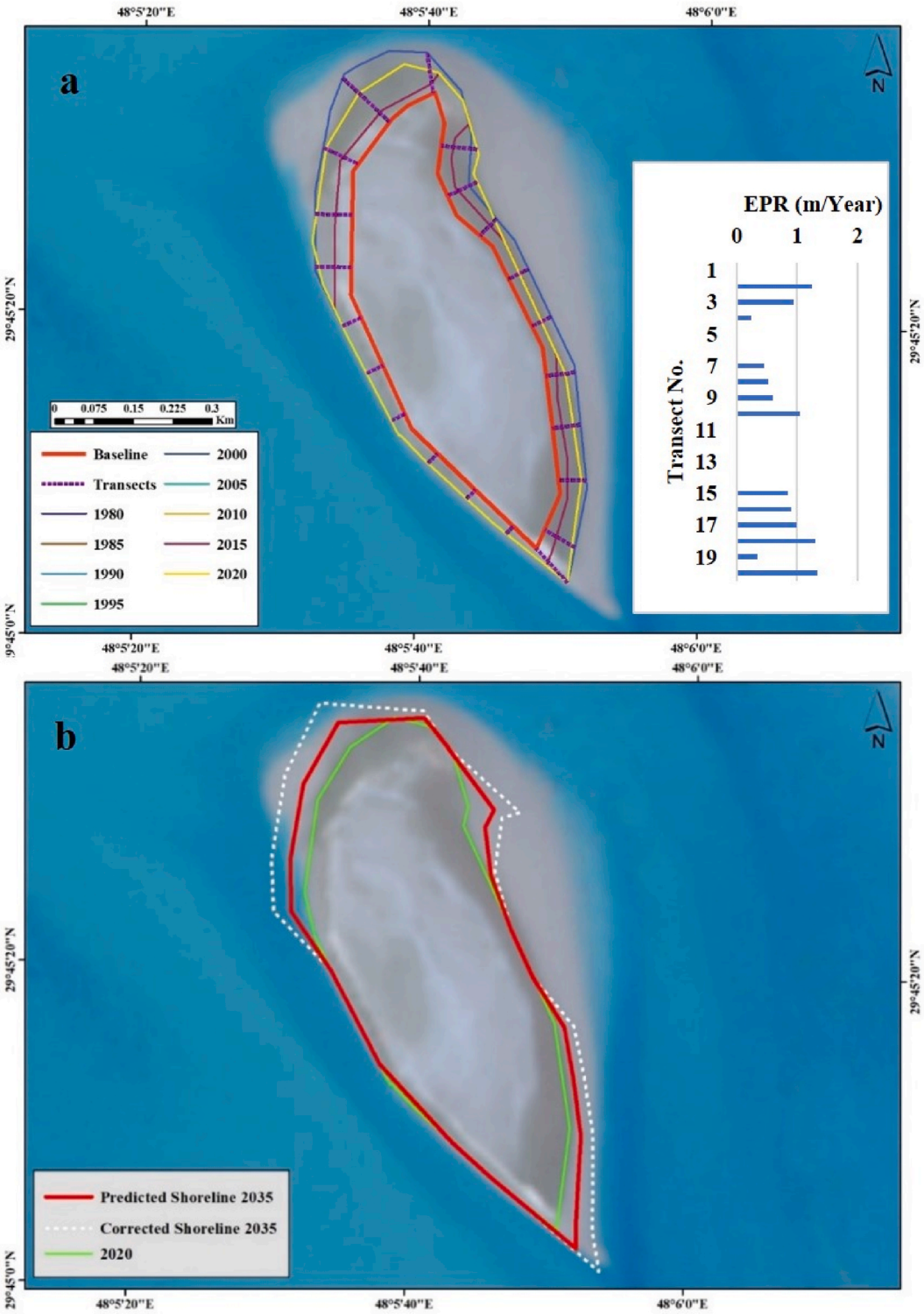


**Fig. 24.** Multitemporal shoreline position of third and fourth island from 1980 to 2020 with transects with EPR, b) Predicted and corrected Shoreline 2035.

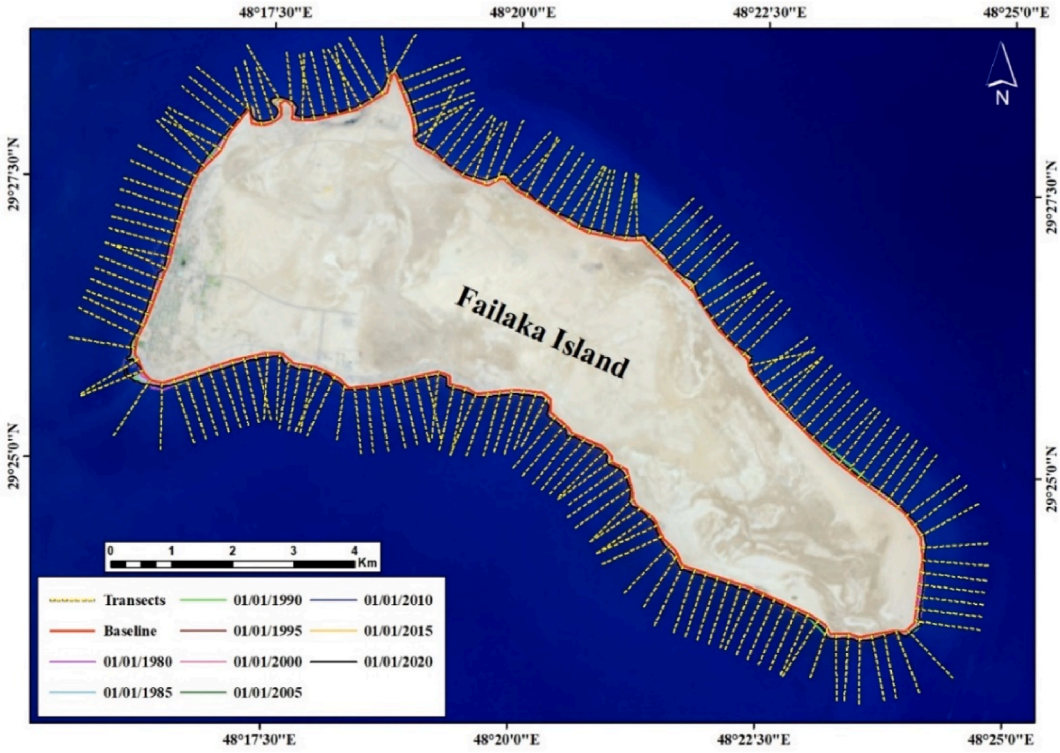


**Fig. 25.** Multitemporal shoreline position of Failaka island from 1980 to 2020 with transects.

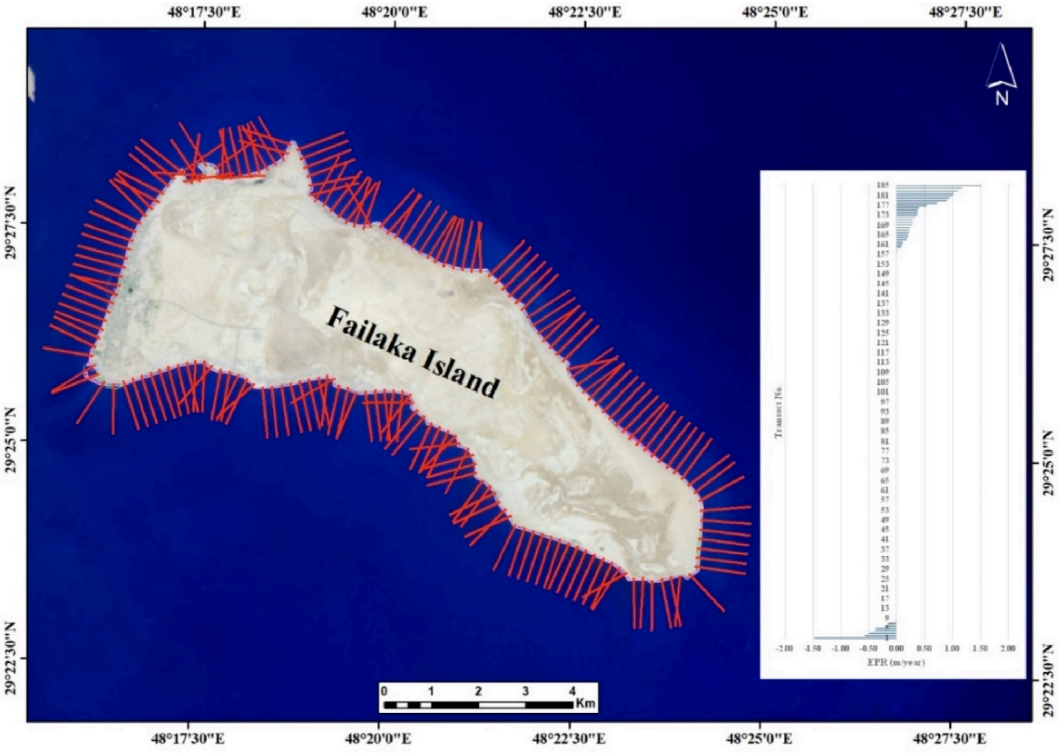


**Fig. 26.** EPR from 1980 to 2020 of Failaka island.

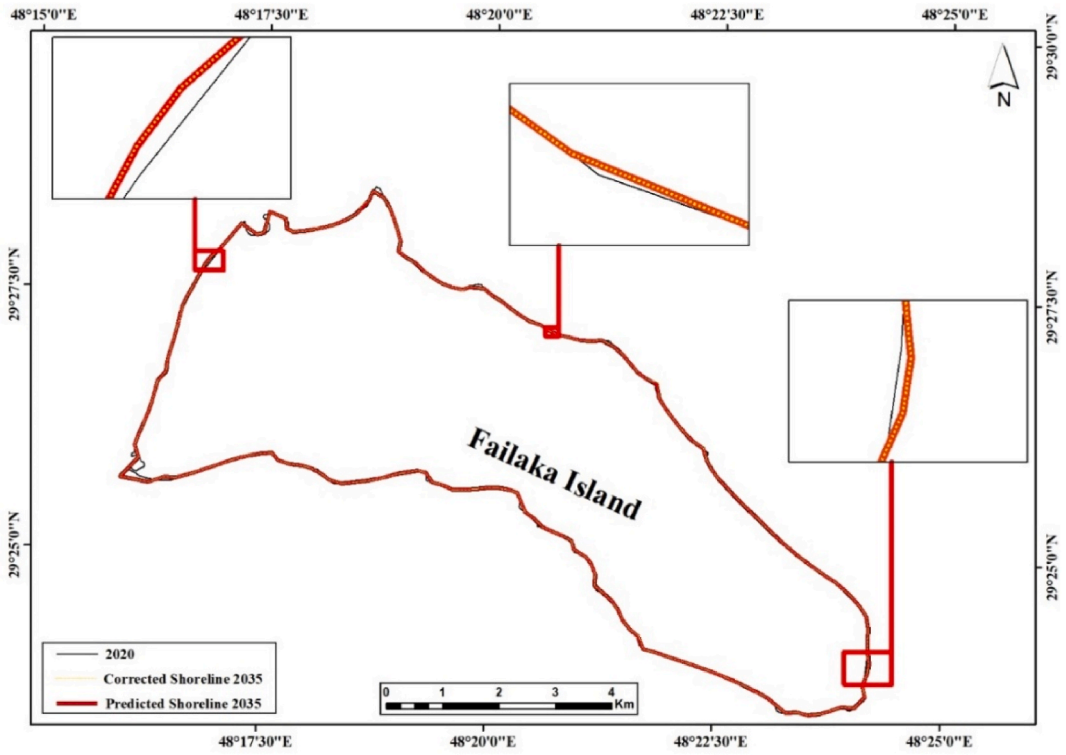


**Fig. 27.** Predicted and corrected Shoreline 2035 of Failaka island.

## 5. Recommendation

The shoreline is highly active. So, compared to medium-resolution satellite data, shoreline delineation from high-resolution satellite data will be more accurate. In this study, the shoreline was predicted using the EPR model. However, other models, such as Net Shoreline Movement, Linear Regression Rate, Weighted Linear Regression Rate, etc., can also be tested. Moreover, coastal protective structures must be established to protect the mainland from rapid coastal erosion.

## Author contribution statement

Ikram M. S. Al-Attar: Conceived and designed the experiments; Analyzed and interpreted the data; Contributed reagents, materials, analysis tools or data; Wrote the paper. Manar A. Basheer: Performed the experiments; Analyzed and interpreted the data; Wrote the paper.

## Data availability statement

Data included in article/supplementary material/referenced in article.

## Declaration of competing interest

The authors declare that they have no known competing financial interests or personal relationships that could have appeared to influence the work reported in this paper.

## References

[1] P.S. Mujabar, N. Chandrasekar, Shoreline change analysis along the coast between Kanyakumari and Tuticorin of India using remote sensing and GIS, Arabian J. Geosci. 6 (3) (2011) 647–664, https://doi.org/10.1007/s12517-011-0394-4.
[2] D.L. Passeri, S.C. Hagen, S.C. Medeiros, M.V. Bilskie, K. Alizad, D. Wang, The dynamic effects of sea level rise on low-gradient coastal landscapes: a review, Earth's Future 3 (6) (2015) 159–181, https://doi.org/10.1002/2015ef000298.
[3] E. Armenio, F. De Serio, M. Mossa, A.F. Petrillo, Coastline evolution based on statistical analysis and modeling, Nat. Hazards Earth Syst. Sci. 19 (9) (2019) 1937–1953, https://doi.org/10.5194/nhess-19-1937-2019.
[4] A.M. Muslim, G.M. Foody, P.M. Atkinson, Localized soft classification for super-resolution mapping of the shoreline, Int. J. Rem. Sens. 27 (11) (2006) 2271–2285, https://doi.org/10.1080/01431160500396741.

[5] R. Dewi, W. Bijker, A. Stein, M. Marfai, Fuzzy classification for shoreline change monitoring in a part of the northern coastal area of java, Indonesia, Rem. Sens. 8 (3) (2016) 190, https://doi.org/10.3390/rs8030190.
[6] M.D. Yang, T.C. Su, C.H. Hsu, K.C. Chang, A.M. Wu, Mapping of the 26 December 2004 tsunami disaster by using FORMOSAT-2 images, Int. J. Rem. Sens. 28 (13–14) (2007) 3071–3091, https://doi.org/10.1080/01431160601094500.
[7] K. Appeaning Addo, P.N. Jayson-Quashigah, K.S. Kufogbe, Quantitative analysis of shoreline change using medium resolution satellite imagery in keta, Ghana, Mar. Sci. 1 (1) (2012) 1–9, https://doi.org/10.5923/j.ms.20110101.01.
[8] S. Maiti, A.K. Bhattacharya, Shoreline change analysis and its application to prediction: a remote sensing and statistics-based approach, Mar. Geol. 257 (1–4) (2009) 11–23, https://doi.org/10.1016/j.margeo.2008.10.006.
[9] K. Nassar, W.E. Mahmod, H. Fath, A. Masria, K. Nadaoka, A. Negm, Shoreline change detection using DSAS technique: case of North Sinai coast, Egypt, Mar. Georesour. Geotechnol. 37 (1) (2018) 81–95, https://doi.org/10.1080/1064119x.2018.1448912.
[10] R. Mani Murali, M. Ankita, S. Amrita, P. Vethamony, Coastal vulnerability assessment of Puducherry coast, India, using the analytical hierarchical process, Nat. Hazards Earth Syst. Sci. 13 (12) (2013) 3291–3311, https://doi.org/10.5194/nhess-13-3291-2013.
[11] M.S. Fenster, R. Dolan, J.F. Elder, A new method for predicting shoreline positions from historical data, J. Coast Res. (1) (1993) 147–171 [online] 9, www.jstor.org/stable/4298075. (Accessed 15 July 2022).
[12] H. Burningham, J. French, Understanding coastal change using shoreline trend analysis supported by cluster-based segmentation, Geomorphology (2017) 131–149, https://doi.org/10.1016/j.geomorph.2016.12.029 [online] 282.
[13] M. Sebat, J. Salloum, Estimate the rate of shoreline change using the statistical analysis technique (EPR), Business & IT VIII (1) (2018) 59–65, https://doi.org/10.14311/bit.2018.01.07.
[14] A. Hassan, M.A. Hassaan, Potential impact of sea level rise on the geomorphology of Kuwait state coastline, Arabian J. Geosci. 13 (21) (2020) 1–16.
[15] N.S. Aladwani, Shoreline Change Rate Dynamics Analysis and Prediction of Future Positions Using Satellite Imagery for the Southern Coast of Kuwait: A Case Study, Oceanologia, 2022.
[16] J.A. Albanai, Spatial distribution of Kuwait coastal geomorphological features using remote sensing methods and GIS soultions, J. Soc. Sci. (2021).
[17] Kuwait EPA, Kuwait National Adaptation Plan 2019–2030: Enhanced Climate Resilience to Improve Community Livelihood and Achieve Sustainability, Kuwait Environmental Public Authority, 2019 (EPA)).
[18] S. Neelamani, S. Uddin, Erosion and accretion index for Kuwaiti coast, Int. J. Environ. Res. 7 (3) (2013) 679–684.
[19] C. Sabarathinam, H. Bhandary, A. Al-Khalid, A geochemical analogy between the metal sources in Kuwait Bay and territorial sea water of Kuwait, Environ. Monit. Assess. 191 (3) (2019) 1–19.
[20] F. Khalaf, M. Al-Hashash, Aeolian sedimentation in the north-western part of the Arabian Gulf, J. Arid Environ. 6 (4) (1983) 319–332.
[21] S. Neelamani, F. Al-Shatti, The expected sea-level rise scenarios and its impacts on the Kuwaiti coast and estuarine wetlands, Int. J. Ecol. Dev. 29 (3) (2014) 32–43.
[22] A.-A. Ikram, S. Noha, M. H, H. E.-G, M. N.E. din, Geospatial ANALYIS for the potential impacts of outfalls discharge on Kuwait, J. Environ. Sci. (China) 44 (1) (2018) 71–91, https://doi.org/10.21608/jes.2018.32160.
[23] F. Picha, Depositional and diagenetic history of Pleistocene and Holocene oolitic sediments and sabkhas in Kuwait, Persian Gulf, Sedimentology 25 (3) (1978) 427–450, https://doi.org/10.1111/j.1365-3091.1978.tb00320.
[24] J. Al-Sulaimi, A. Mukhopadhyay, An overview of the surface and near-surface geology, geomorphology, and natural resources of Kuwait, Earth Sci. Rev. 50 (3–4) (2000) 227–267, https://doi.org/10.1016/s0012-8252(00)00005-2.
[25] A. El-kaṣaby, Human Effects on the Geomorphology of Kuwait State's Coasts, Center for research and studies of Kuwait, Kuwait, 2014.
[26] M. Al Sarawi, F. El Baz, M. Koch, Geomorphologic controls on surface deposits of Kuwait as depicted in satellite images, Kuwait J. Sci. Eng. 33 (2) (2006), 123145.
[27] H. Tang, A. Al-Dousari, Air pollution background study in Boubyan Island of Kuwait, Int. J. Sustain. Dev. Plann. 1 (3) (2006) 326–341, https://doi.org/10.2495/sdp-v1-n3-326-341.
[28] S. As Omar, R. Grina, Sustainable land use planning for bubiyan island in Kuwait. Informatics for environmental protection-networking environmental information, 1996, in: M.A. Al-Sarawi, Y.R. Marmoush, J.-M. Lo, K.A. Al-Salem (Eds.), Coastal Management of Failaka Island, Kuwait. Journal of Environmental Management, vol. 47, 2005, pp. 299–310, https://doi.org/10.1006/jema.1996.0055, 4.
[29] S. Patitucci, G. Uggeri, Failakah, insediamenti medievali islamici: ricerche e scavi nel Kuwait, Bretschneider, Cop, Roma, 1984.
[30] E.R. Thieler, E.S. Hammar-Klose, National assessment of coastal vulnerability to sea-level rise; preliminary results for the U.S. Pacific Coast, Open File Rep. (2000), https://doi.org/10.3133/ofr00178.
[31] S.B. Elkafrawy, M.A. Basheer, H.M. Mohamed, D.M. Naguib, Applications of remote sensing and GIS techniques to evaluate the effectiveness of coastal structures along Burullus Headland-Eastern Nile Delta, Egypt, The Egyptian Journal of Remote Sensing and Space Science 24 (2) (2021) 247–254.
[32] E.R. Thieler, E.S. Hammar-Klose, National assessment of coastal vulnerability to sea-level rise, U.S. Atlantic Coast. Open-File Report (1999), https://doi.org/10.3133/ofr99593.
[33] E.A. Himmelstoss, in: E.R. Thieler, E.A. Himmelstoss, J.L. Zichichi, Ayhan Ergul (Eds.), DSAS 4.0 Installation Instructions and User Guide, 2009, 2008-1278.
[34] E.A. Himmelstoss, R.E. Henderson, M.G. Kratzmann, A.S. Farris, Digital Shoreline Analysis System (DSAS) Version 5.0 User Guide (No. 2018-1179), US Geological Survey, 2018.
[35] P.N. Ojukwu, Evaluating Long-Term Shoreline Change in Dakar (Senegal) Using Satellite Data (Master's Thesis, University of Twente, 2021.